Nuclear Flow and Particle Production Near 1 AGeV: Recent Results from the FOPI Collaboration

J. RITMAN
II. Phys. Inst., Heinrich-Buff-Ring 16, D-35392, Gießen Germany
for the **FOPI** collaboration

The FOPI collaboration at GSI/Darmstadt is collecting data on heavy ion collisions over a wide range of system size and beam energy. Systematic studies of very central collisions reveal that a large fraction of the initial energy is converted into a collective radial expansion showing a dependence on the system size. With increasing beam energy particle production also becomes an important component of the energy balance. At beam energies near the free production threshold of the strange quark containing kaons, the production and propagation of these particles are expected to maintain sensitivity to bulk nuclear matter properties such as the equation of state and whether hadronic masses suffer modifications in a dense nuclear environment. Recent results from nuclear flow studies, as well as pion and kaon production measurements are presented.

1 Introduction

The only method available to study a dense, strongly interacting system in a controlled laboratory environment is to measure relativistic heavy ion collisions. Of particular interest is the determination of the bulk compressibility of nuclear matter as well as whether or not hadronic properties are modified in a dense baryonic environment. In order to study these effects it is essential to determine as completely as possible the complete phase space distribution of the reaction products from the heavy ion collision. Therefore, the FOPI collaboration has built a large acceptance spectrometer to measure fixed target experiments with heavy ions beams delivered the SIS accelerator at GSI Darmstadt.

2 Detector Capabilities

The FOPI detector is a highly modular system of several sub-detectors which provide charge and mass separation over nearly the full 4π solid angle [1, 2]. These detectors provide charge and mass determination with almost complete azimuthal symmetry. Momentum determination is achieved by measuring the particles rigidity in a 0.6 T magnetic field produced by a Superconducting Solenoid with an inner diameter of 2.4 m and a length of 3.3 m. In the forward direction, the highly segmented Forward Wall (FW) covers the polar angles between $1^\circ < \Theta_{Lab} < 30^\circ$. The 764 Scintillator strips provide energy loss ΔE and position information in addition to a Time–of–Flight (ToF) measurement, thus allowing velocity and charge determination. Within the range $7^\circ < \Theta_{Lab} < 28^\circ$ the particle's momentum is also measured by the HELITRON drift chamber.

At backward angles the particle tracking is performed by the Central Drift Chamber (CDC), a cylindrical tracking detector covering an additional range in polar angle of $32^\circ < \Theta_{Lab} < 150^\circ$. The CDC is a drift chamber of the jet type which operates at atmospheric pressure and is 200 cm long with inner and outer radii of 20 and 80 cm respectively. In order to enhance the particle identification capabilities of the CDC, the tracks are extrapolated to the Scintillator and Cherenkov array (Barrel) that surrounds the CDC and matched with the appropriate Barrel hit. The Barrel covers the polar angular range of $38^\circ < \Theta_{Lab} < 160^\circ$. The velocity is determined by dividing the path length as measured with the CDC by the ToF from the Barrel.

As a typical example of the resolution achievable in the backward hemisphere with the CDC-Barrel combination, the particle's charge (determined from velocity and the specific energy loss $< dE/dx >$) is plotted as a function of the reconstructed mass divided by charge (from the rigidity and velocity) in Figure 1. This data which

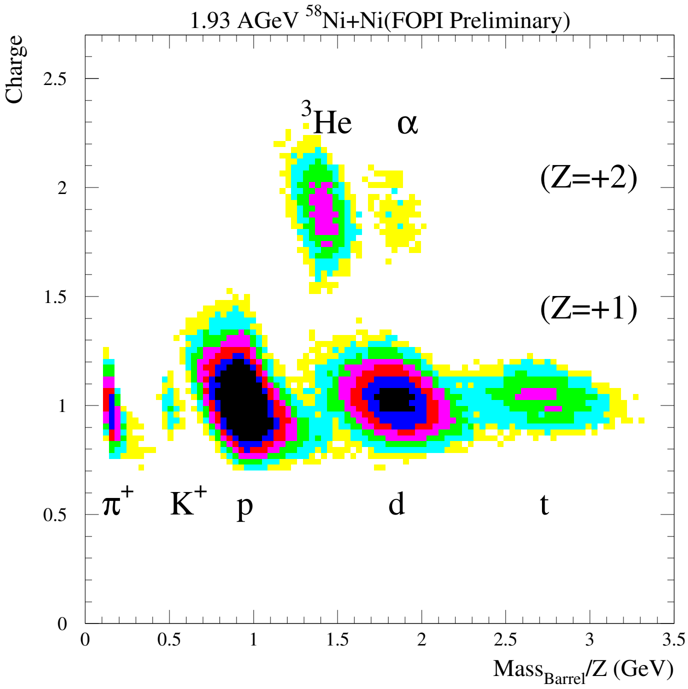

Figure 1: Reconstructed charge from $< dE/dx >$ and velocity as a function of the particle's mass divided by charge from the rigidity and velocity.

was collected in the system 1.93 AGeV $^{58}Ni +^{58} Ni$ is displayed with a logarithmic intensity scale. It can be seen that particles of different charge are very well separated as well as the different isotopes of a given ion species. Furthermore, mesons such as the positive pions and kaons are seen to be cleanly separated in this representation. In order to produce these results, very sophisticated tracking and matching algorithms have been developed which allow the track information to be reconstructed from the several thousand single detector hits produced in a typical event.

In addition to detecting charged particles, the FOPI detector is also able to measure certain neutral particles (those which decay into charged particle). In particular, particles with strange quark content can be identified via the invariant mass (M_{inv}) of decay products. For instance, the K^0_S and Λ particles have sizable decay probabilities into $\pi^+\pi^-$ and $\pi^- p$ respectively. Due to their strange quark content, the K^0_S and Λ have lifetimes $c \cdot \tau$ of 2.7 and 7.9 cm respectively, thus allowing the combinatorial background to be greatly reduced by only selecting candidate track pairs that intersect to form a secondary vertex away from the primary event vertex. Figures 2 and 3 show the M_{inv} spectra for K^0_S, and Λ, candidates (points) as well as the mixed event background (solid lines). Gaussian fits to the data after background

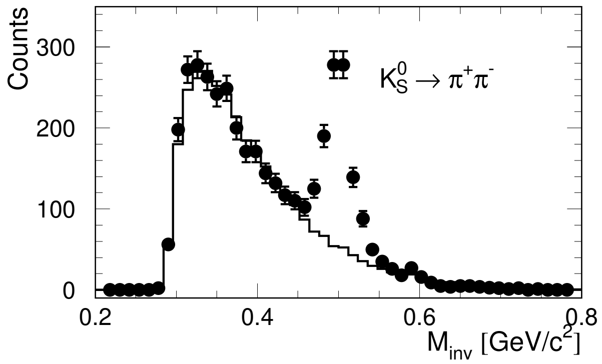

Figure 2: The points show the invariant mass spectrum of $\pi^+\pi^-$ pairs which fulfill the K^0_S hypothesis, the mixed event background is denoted by the solid line. After background subtraction the peak has a width of $\sigma = 16$ MeV/c^2.

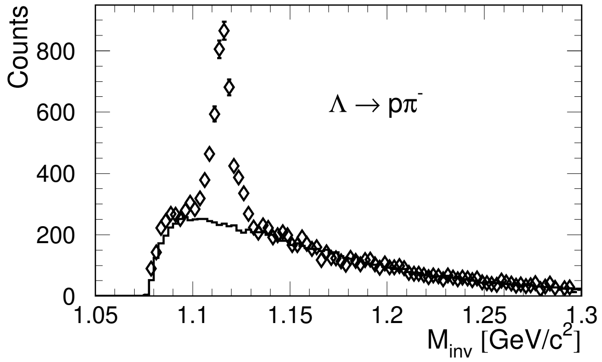

Figure 3: The points display the invariant mass spectrum of $p\pi^-$ pairs which fulfill the Λ, conditions, the mixed event background is denoted by the solid line. After background subtraction the peak has a width of $\sigma = 5$ MeV/c^2.

subtraction have widths (σ) of 16 and 5 MeV/c^2 respectively. The ratio of the yield in the peak to the total yield (integrated over a range of $\pm 2\sigma$ from the peak location) is 75%(K_S^0) and 60%(Λ).

Furthermore, pairs of charged kaons can be used to identify the Φ meson, as shown in Figure 4. The upper panel in this figure shows the invariant mass distribution of the K^+K^- pairs for a total of 6×10^6 central events of 1.93 AGeV $^{58}Ni + ^{58}Ni$ which demonstrates a significant peak at the Φ mass above the mixed event background which is shown as the solid distribution. The lower panel shows the distribution after background subtraction. The solid line denotes a Gaussian fit with width $\sigma = 7$ MeV/c^2 which is dominated by the detector resolution.

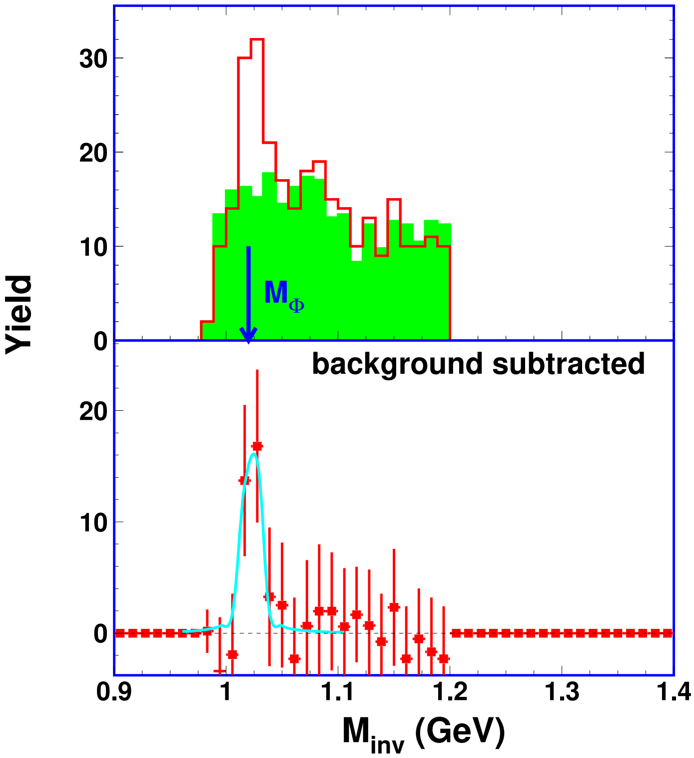

Figure 4: The upper panel shows the invariant mass distribution of K^+K^- pair and the solid histogram shows the mixed event background. After background subtraction, the lower panel displays a peak associated to the Φ meson.

3 Nuclear Flow

When using relativistic heavy ion collisions to produce a volume of hot, compressed nuclear matter, a very important aspect that needs to be understood is to what extent the nuclei are stopped and how much of the initial kinetic energy of the incoming nuclei is transformed into a mid-rapidity source with the available phase space being evenly populated.

In nuclear collisions above circa 100 AMeV with medium impact parameters (i.e. roughly half the nuclear diameter) the large fraction of the projectile and target nucleons that are not in the geometrical overlap region (spectators) are less effected by the collision than those in the overlap region (participants). At mid-rapidity this effect is apparent by the existence of an azimuthal asymmetry (squeeze-out) which is related to absorption of particles from the participant region by the spectator matter [3, 4]. This asymmetry is clearly seen in Figure 5, which displays the mid-rapidity azimuthal distributions ($dN/d\phi$) of deuterons in the system Au+Au. The different symbols (from bottom to top) correspond to beam energies of 90, 120, 150, 250, and 400 AMeV. These results were collected for events with an impact parameter of roughly half the nuclear diameter, and have been restricted to the same range of scaled transverse momentum ($p_t^{(0)} = p_t/m/(p_{\rm beam}/m_{\rm beam})$) in order to be able to compare the results at the different energies. Not only is the magnitude but also the sign of the asymmetry seen to change in these data, thus reflecting changes in the relative balance of the attractive mean-field to the Coulomb and repulsive nucleon-nucleon forces.

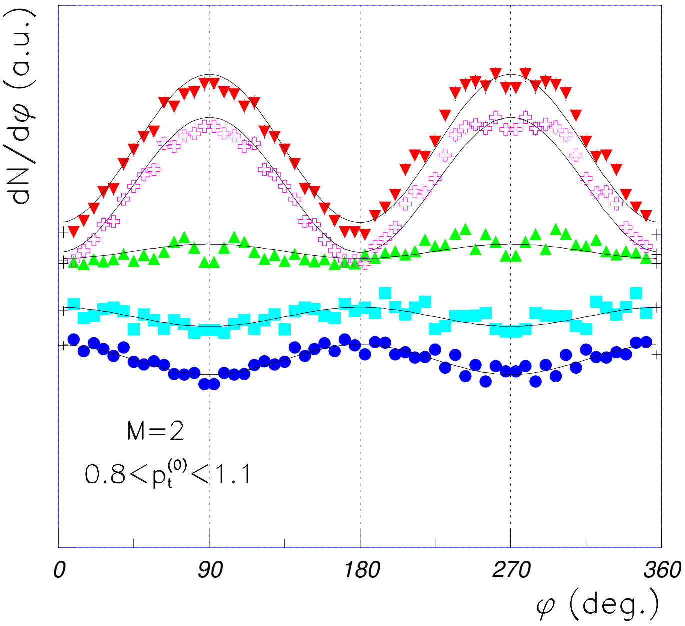

Figure 5: Azimuthal distributions of deuterons at mid-rapidity from the system Au+Au within a range of scaled transverse momentum for beam energies ranging from 90 (filled circles) to 400 AMeV (filled triangles).

With increasing centrality (i.e. decreasing impact parameter) the azimuthal asymmetry is seen to vanish. This change in the event topology is coupled with a narrowing of the rapidity distribution indicating that a larger fraction of the incoming nuclei's ordered longitudinal energy is converted to stochastic motion of the nucleons involved in the collision. To more precisely address the question of how complete the nuclear stopping is, the system size dependence of the produced fragment's phase space distribution has been studied in central collisions at 250 AMeV. In particular, the rapidity density distributions of fragments up to charge 6 are shown in Figure 6 as a function of scaled rapidity ($Y^{(0)} = Y_{lab}/Y_{CM} - 1$) for the most central 3% of events in a light, medium, and a heavy system each at 250 AMeV. Here it is observed that the rapidity distributions of all fragments species from the light systems are considerably elongated, which implies that even for central collisions of

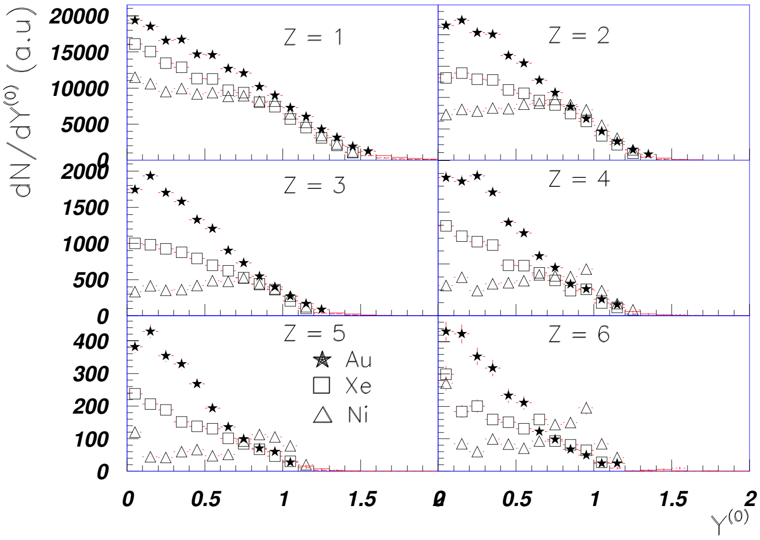

Figure 6: Rapidity density distributions as a function of scaled rapidity ($Y^{(0)} = Y_{lab}/Y_{CM} - 1$) for fragments with charge Z=1 to 6. The data were collected for the most central 3% of events at 250 AMeV and the star, square, and triangle symbols correspond to the systems Au, Xe, and Ni, respectively.

light ions such as Ni there is significant transparency. With increasing system size the rapidity distributions become more and more concentrated at mid-rapidity, thus indicating that a larger fraction of the beam's initial kinetic energy has been expended in heating and compressing the nuclear matter in the collisional zone. Not until the largest system size is reached (Au) do the rapidity distributions resemble that of isotropic emission as discussed in detail in reference [5].

For such central events, it has been observed that the mean kinetic energy of the produced particles rises with increasing mass [6]. This behavior has been interpreted as a collective radial expansion. As a results of this radial flow, less energy is available to the system for the stochastic motion (temperature), thus this energy must be properly accounted for when attempting to describe for the particle abundances via thermal models. As an example of the importance of this radial flow, the results of several experiments are collected in Figure 7. Here results based upon an analysis of the light particle spectra of Au+Au from the FOPI (filled triangles) [7] and EOS (open circles) [8] collaborations are presented in comparison with the light particle results in Ni from FOPI (filled circles) [9]. The open squares represent the results when heavy clusters ($Z \leq 12$) [5] are analyzed using a broad flow velocity profile rather than a shell-type freeze-out as was used for the light particle analyses. These differences lead to a larger mean flow velocity (and correspondingly smaller "temperature") in the heavy fragment analysis, thus indicating the systematic uncertainty inherent in this type of analysis. Nevertheless, a trend is quite clear that with increasing beam energy both the "temperature" and the mean flow velocity ($< \beta_r >$) increase. In fact the "temperature" value extracted appears to be independent of the system size while the radial flow is significantly lower in the nickel system than in gold. The increase in the radial expansion (blast) for the heavy system is directly correlated with the increased stopping (see Fig. 6) and possibly indicates that the heavier system has obtained a higher central density during the initial stages of the reaction.

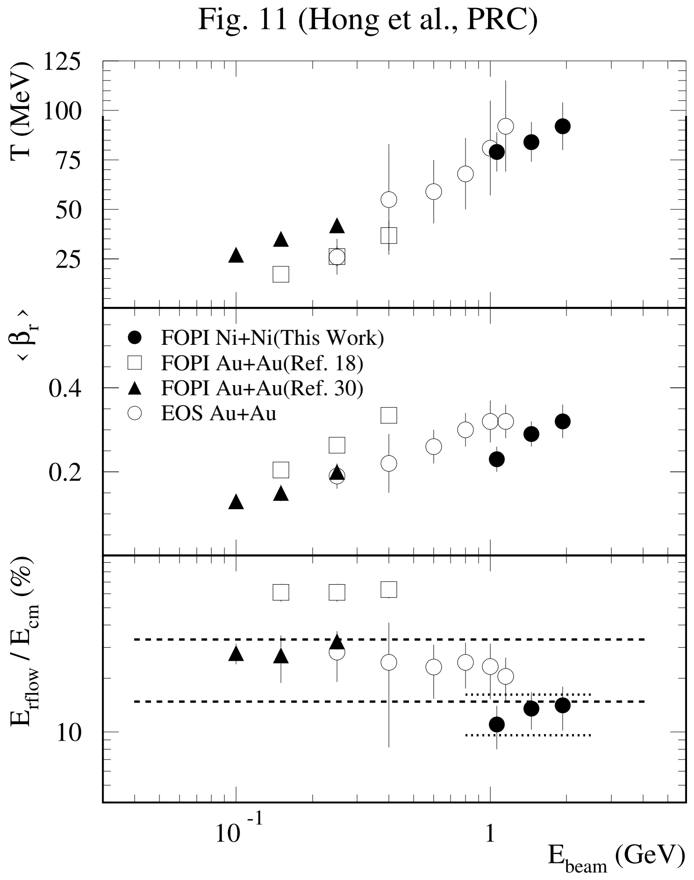

Figure 7: The upper two panels show a compilation of the extracted temperature and radial flow velocity parameters as a function of beam energy. The lowest panel shows the ratio of the radial flow energy to the total energy available in the system.

4 Strangeness Production

With increasing beam energy particle production (mostly pions) also becomes an important factor in the energy balance of the collisional system. However, due to the large absorption cross section, pion production is primarily sensitive to the conditions near freeze-out. In contrast, near threshold production of $s\overline{s}$ quark pairs should remain sensitive to the prevailing conditions at the moment of production because of the conservation of strangeness. Since the $s\overline{s}$ production channel with the lowest threshold is the associated production of a K^+ meson with a hyperon and the K^+ has a small elastic cross section with nucleons, the yield and phase space density of K^+ mesons are expected to retain information about the initial hot and dense stage of the collision. Thus the K^+ should be a useful probe to help determine the nuclear equation of state and/or whether hadronic properties are effected in a high baryon density environment.

Within this context the K^+ phase space distribution has been analyzed in the system ^{58}Ni+^{58}Ni at 1.93 AGeV. For central events (most central 350 mb) the kaon phase space distribution is quite isotropic in the azimuthal degree of freedom [10]. The longitudinal and transverse degrees of freedom have been analyzed by studying the transverse mass spectra for several narrow slices in rapidity [11]. In each rapidity interval the data are well described by a Boltzmann-type function from which the slope (T_B) and yield ($dN/dy^{(0)}$) are determined as a function of rapidity. For comparison, the proton and π^- spectra have also been studied in a similar fashion [9].

While the protons can be well described by a single exponential in all rapidity intervals, the pion's spectra exhibit a concave shape, which can be described by the sum of two such exponential functions with inverse slope parameters T_B^L and T_B^H for the softer and stiffer components, respectively. The inverse slope parameters of the K^+, protons, and both pion components are plotted together in Figure 8 for the different rapidity slices. The symbols of the left indicate the measured data which have been reflected onto the right side for symmetry reasons. At midrapidity the proton slopes are higher than the pion's as expected for a system with a a collective expansion velocity. The magnitude of the K^+ slopes near target rapidity is similar to or lower than the proton slopes, which is qualitatively in agreement with the midrapidity results from the KaoS collaboration [12], but in contrast to the somewhat harder K^+ spectra than for protons as obtained by Schnetzer et al. in the system Ne+NaF at 2.1 AGeV [13].

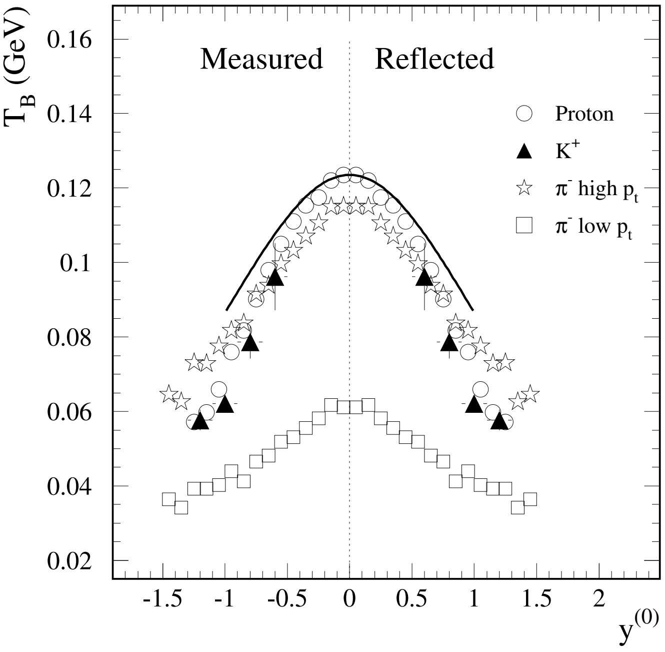

Figure 8: Measured slope parameters of π^-, K^+, and protons as a function of normalized rapidity for the system $^{58}\mathrm{Ni}+^{58}\mathrm{Ni}$ at 1.93 AGeV. The solid line marks the expected behavior of a thermal source with a temperature given by the proton's midrapidity slope.

Away from midrapidity ($y^{(0)} = 0$) the measured inverse slope parameters T_B of all particles decrease with increasing $|y^{(0)}|$. For an isotropic thermal source of temperature T, the T_B values possess the following functional dependence on rapidity:

$$T_B = T/cosh(y). \tag{1}$$

For the pions, the rapidity distribution of the T_B^H values follow the function in Eq. 1 for $|y^{(0)}| < 1$, in agreement with isotropic emission from a source at midrapidity. This shape however is rather insensitive to the presence or absence of radial flow due to the small pion mass. In contrast, the pion's T_B^L distribution is somewhat flatter than expected from Eq. 1, which is in agreement with suggestions that this component is governed primarily by the decay kinematics of the Δ resonance [14]. On the other hand, the proton T_B distribution (open circles) is noticeably narrower than the $T/cosh(y)$ dependence which is shown by the solid line in Fig. 8, thus indicating a more complex source behavior. The K^+ T_B distribution has a similar form to that of the protons indicating significant elastic $\mathrm{K}^+\mathrm{N}$ scattering.

The kaon rapidity distribution has been determined by integrating the Boltzmann functions that have been fit to the data and the results are presented in Figure 9 together with the π^- and proton results. Again the measured points on the left side have been reflected around midrapidity. The dashed lines represent the expected distribution for a purely thermal source located at midrapidity, and the solid lines shown in this figure represent the expected distribution for a radially expanding thermal source [15]. In this case the temperature (T=92 MeV) and flow velocity (β=0.32) parameters were determined by a simultaneous fit to the π^-, proton, and deuteron midrapidity spectra [9] and the yield was normalized to the data.

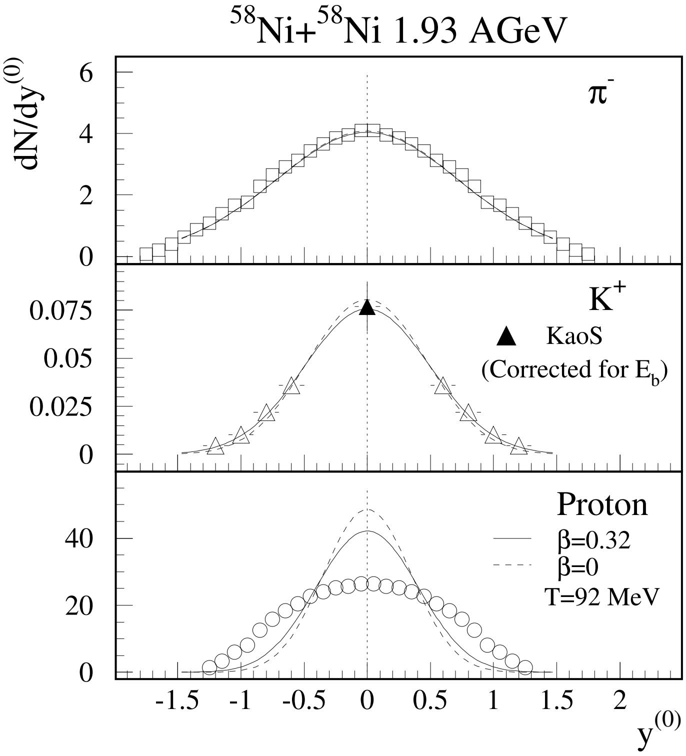

Figure 9: Deduced multiplicity density dN/dy$^{(0)}$ of pions, kaons, and protons for the system ^{58}Ni+^{58}Ni at 1.93 AGeV. The data points to the right of the dashed line are reflections of the points on the left.

The $dN/dy^{(0)}$ distributions for the produced particles (π^- and K^+) are well reproduced by the two curves showing a thermalized source both with and without a radial flow component. In contrast, the non-thermal behavior of the protons is very noticeable. This may result from significant transparency or so called “Halo” effects resulting from the coarse centrality selection Ni+Ni due to the large multiplicity fluctuations in this rather small system.

To determine the total kaon yield the form of the dN/dy spectrum has been taken from that of a radially expanding source as mentioned above and shown by the solid line in Fig. 9. In justification of this assumption, the mid-rapidity data from the KaoS collaboration for an equivalent centrality has been included after correcting for the different beam energy (1.8 AGeV). The excitation function of the total K$^+$ multiplicity in the central events studied here is presented in Fig. 10. In order to facilitate the comparison of these exclusive results with other experimental data, the yield is expressed relative to the mean number of participating nucleons $< A_{part} >$.

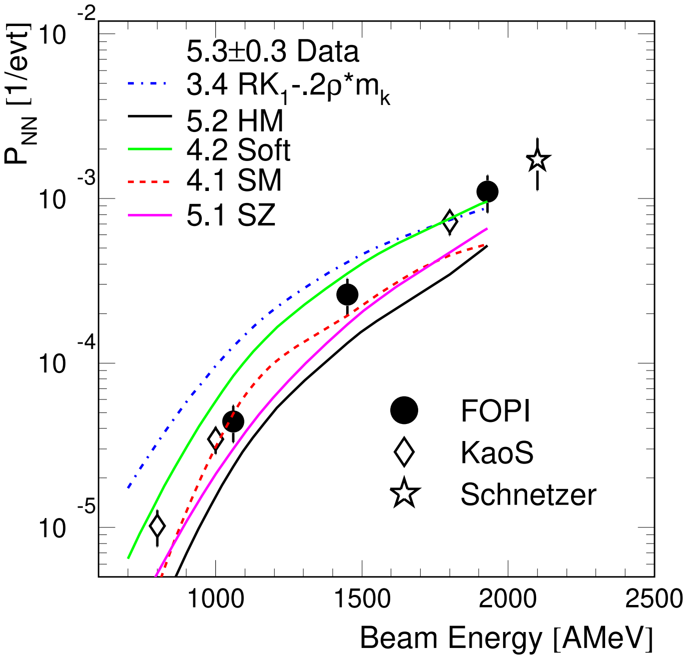

Figure 10: Kaon excitation function. The kaon production probability is presented normalized to the number of participating nucleons. The various curves correspond to calculations with the IQMD model employing different parameterizations for the equation of state. The numbers correspond to the exponent α from Eq. 2 that have been fit to the respective distribution.

For comparison, these data values have been plotted together with the Ni + Ni results from the KaoS collaboration [12]. The KaoS results which were obtained in a narrow window at mid-rapidity have been scaled by the reaction cross section (2.71 b) and by the mean number of participating nucleons, which is $A_{proj}/2$ for an inclusive measurement of a symmetric system within a geometric model [16]. Although this normalization of the yield by $< A_{part} >$ is quite successful for pions in small and medium mass systems [17], for large systems (Au) at sub-threshold energies [18] this ratio does vary with centrality for K$^+$ mesons. Also plotted in this figure is the expected excitation function as calculated with the IQMD model for several different parameterizations of the equation of state [19]. Since the *absolute* magnitude of the calculated yield is sensitive to various factors such as which parameterizations of the elementary cross-sections have been used as well as which baryonic resonances have been taken into account, a direct comparison of the data to the model results here is limited to the *relative* rise with increasing beam energy.

The data are well described by a fit with a function of the following type:

$$P_{NN}^{K^+} \propto E_{BEAM}^{\alpha} \tag{2}$$

where the exponent is $\alpha = 5.3 \pm 0.3$. The exponents α for these various calculations are listed in the figure. The first parameterization shows the expected behavior when a density dependent kaon mass is employed. Although this Ansatz has been suggested as an important mechanism in order to explain the large sub-threshold kaon yield, the absolute magnitude is quite uncertain as discussed above and the predicted excitation function is much too flat to be consistent with the data. The soft equation of state has been used both with and without a momentum dependent interaction (SM and Soft, respectively). In both cases the excitation function is steeper than the density dependent mass, however neither can reproduce the strong rise observed in the data. Much better agreement is obtained for the soft EOS when the Zwermann parameterization of the elementary cross section is used. This parameterization however rises too strongly at higher values of $\sqrt{s}$, thus leading to an artificially large exponent α. Thus the only parameterization that adequately reproduces the relative rise of the kaons excitation function is the hard EOS with momentum dependence (HM). This EOS has an absolute kaon yield that is lower than the data by about a factor 2 which is roughly the uncertainty in the calculations due to the factors mentioned above. Although this conclusion is in contrast to that of previous studies, they have generally been limited to a single system at one beam energy.

Furthermore, additional constraints to the in-medium behavior of kaons are available to the FOPI collaboration by an analysis of the kaon's sideward flow. This signal has been suggested to be sensitive to the mean potential felt by the kaons [20]. In fact, previous results [10] from the FOPI collaborations reveal that the positive kaons have a very small sideward flow profile which is significantly different from that of the coproduced Λ baryons. These results are consistent with the predicted flow pattern when the kaons are subject to both vector and scalar potentials. Newer results with a factor 10 more statistics are currently being analyzed to determine the centrality dependence of the sideward flow signal as well as the shape of the negative kaon's flow pattern.

5 Summary and Outlook

In this talk a collection of recent results from the FOPI collaboration has been presented. The mid-rapidity azimuthal distributions of deuterons clearly show a change of sign between 120 and 150 AMeV. This behavior is a sensitive testing ground of the compressibility of nuclear matter. With increasing system size the rapidity distributions become more compact, and not until the largest system is reached (Au) does the phase space distribution achieve a roughly isotropic form in central collisions. The question of nuclear stopping is very important in order to understand how much of the projectile's initial energy is converted to compressional and thermal energy of the mid-rapidity source.

From the analysis of light particle spectra the freeze-out conditions have been parameterized in terms of a collective radial expansion velocity and a stochastic component. The fraction of energy contained in the expansion is sensitive to the form of the velocity (i.e. freeze-out density) profile used. From the light particle spectra both the “temperature” and the radial flow velocity rise with increasing beam energy such that for a given system size a constant fraction of the initial energy is consumed by the expansion. Furthermore it is observed that although the “temperature” is independent of the system size, the fraction of energy in the expansion decreases with decreasing system size as one might expect since the lighter systems exhibit less stopping.

With increasing energy the production of particles with strange quark content begins to play a significant role. The kaon transverse spectra are similar to the proton's, consistent with substantial thermal relaxation. From the longitudinal motion, a roughly isotropic kaon distributions is deduced, in contrast to the elongated proton distribution due to a significant contribution from spectator nucleons. The total yield exhibits a very sharp rise with beam energy. After considering the uncertainties involved in the absolute magnitude of model calculations of the total kaon yield, the sharp rise of the excitation function seem to be best explained by a stiffer equation of state.

These results represent just some of the analysis activities currently being performed with data taken from the FOPI detector at GSI. These and numerous other FOPI results to be released shortly combine to form a detailed picture of the state of hadronic matter produced in heavy ion collisions in the 0.2 to 2 AGeV region.

Acknowledgments

This work was in part supported by BMBF grant 06 GI 475 I (3).

References

[1] A. Gobbi et al., Nucl. Inst. Meth. 324 (1993) 156.

[2] J. Ritman, Nucl. Phys. B 44 (1995) 708.

[3] V. Ramillien et al., Nucl. Phys. A587 (1995) 802.

[4] N. Bastid et al., submitted to Nucl. Phys. A.

[5] W. Reisdorf et al., Nucl. Phys. A612 (1997) 493.

[6] S. C. Jeong et al., Phys. Rev. Lett 72 (1994) 3468.

[7] G. Poggi et al., Nucl. Phys. A586 (1995) 755.

[8] M. A. Lisa et al., Phys. Rev. Lett. 75 (1995) 2662.

[9] B. Hong et al., submitted to Nucl. Phys. A.

[10] J. L. Ritman et al., Z. Phys. A 352 (1995) 355.

[11] D. Best et al., to be submitted to Nucl. Phys. A.

[12] P. Senger, Proceedings of Meson '96, May 1996, Cracow;
W. Ahner et al., Phys. Lett. B in print.

[13] S. Schnetzer et al., Phys. Rev. Lett. 49 (1982) 989,
ibid Phys. Rev. C 40 (1989) 640.

[14] J. Sollfrank, P. Koch, and U. Heinz, Z. Phys C52 (1991) 593;
G. E. Brown, J. Stachel, and G. M. Welke, Phys. lett. B253 (1991) 19.

[15] P. Siemens and J. O. Rasmussen, Phys. Rev. Lett. 42 (1979) 880.

[16] H. Nifenecker and J. P. Bondorf, Nucl. Phys. A442 (1985) 478.

[17] J. W. Harris et al., Phys. Rev. Lett. 58 (1987) 463.

[18] D. Miskowiec et al., Phys. Rev. Lett. 72 (1994) 3650.

[19] C. Hartnack, priv. comm.

[20] G. Q. Li, C. M. Ko and B. A. Li, Phys. Rev. Lett. 74 (1995) 235.